Journal of Controlled Release 301 (2019) 110–118

Contents lists available at ScienceDirect

Journal of Controlled Release

journal homepage: www.elsevier.com/locate/jconrel

cRGD-decorated biodegradable polytyrosine nanoparticles for robust encapsulation and targeted delivery of doxorubicin to colorectal cancer *in vivo*

Xiaolei Gu, Yaohua Wei, Qianyi Fan, Huanli Sun, Ru Cheng, Zhiyuan Zhong*, Chao Deng*

Biomedical Polymers Laboratory, and Jiangsu Key Laboratory of Advanced Functional Polymer Design and Application, College of Chemistry, Chemical Engineering and Materials Science, and State Key Laboratory of Radiation Medicine and Protection, Soochow University, Suzhou 215123, China

ARTICLE INFO

Keywords:
Polypeptide
Enzyme-responsive
Biodegradable nanoparticles
SPECT/CT imaging
Targeted cancer therapy

ABSTRACT

The clinical success of nanomedicines demands on the development of simple biodegradable nanocarriers that can efficiently and stably encapsulate chemotherapeutics while quickly release the payloads into target cancer cells. Herein, we report that cRGD-decorated biodegradable polytyrosine nanoparticles (cRGD-PTN) boost encapsulation and targeted delivery of doxorubicin (DOX) to colorectal cancer *in vivo*. The *co*-assembly of poly (ethylene glycol)-poly(L-tyrosine) (PEG-PTyr) and cRGD-functionalized PEG-PTyr (mol/mol, 80/20) yielded small-sized cRGD-PTN of 70 nm. Interestingly, cRGD-PTN exhibited an ultra-high DOX encapsulation with drug loading contents ranging from 18.5 to 54.1 wt%. DOX-loaded cRGD-PTN (cRGD-PTN-DOX) was highly stable against dilution, serum, and Triton X-100 surfactant, while quickly released DOX in HCT-116 cancer cells, likely resulting from enzymatic degradation of PTyr. Flow cytometry, confocal microscopy and MTT assays displayed that cRGD-PTN-DOX was efficiently internalized into $\alpha_v\beta_5$ overexpressing HCT-116 colorectal cancer cells, rapidly released DOX into the nuclei, and induced several folds better antitumor activity than non-targeted PTN-DOX and clinically used liposomal DOX (Lipo-DOX). SPECT/CT imaging revealed strong tumor accumulation of ^{125}I-labeled cRGD-PTN, which was 2.8-fold higher than ^{125}I-labeled PTN. Notably, cRGD-PTN-DOX exhibited over 5 times better toleration than Lipo-DOX and significantly more effective inhibition of HCT-116 colorectal tumor than non-targeted PTN-DOX control, affording markedly improved survival rate in HCT-116 tumor-bearing mice with depleting side effects at 6 or 12 mg DOX equiv./kg. cRGD-PTN-DOX with great simplicity, robust drug encapsulation and efficient nucleic drug release appears promising for targeted chemotherapy of colorectal tumor.

1. Introduction

Colorectal cancer remains one of the leading causes of cancer-related death worldwide [1,2]. Surgery is the primary therapeutic strategy for colorectal cancer, however, nearly half of the patients have recurrence and metastasis after resection [3,4]. Chemotherapy based on fluorouracil, capecitabine, oxaliplatin, and irinotecan although has been routinely employed in the clinics for the treatment of colorectal cancer, often exhibits drug resistance and pronounced toxicity to healthy organs [5,6]. Nanomedicines hold great promise in increasing therapeutic efficacy while decreasing adverse effects of chemical drugs [7–9]. Interestingly, liposomal irinotecan (Onivyde®) and liposomal oxaliplatin (Lipoxal) have already been approved or advanced into clinical trials to treat colorectal cancer [10,11]. None of these nanomedicines, however, demonstrate decent colorectal cancer cell selectivity.

The past decade has witnessed vast development of targeted cancer nanomedicines [12–14]. Nanosystems based on biodegradable polyesters and polypeptides have received particular interests [15–20], because of their proven safety. For targeted therapy, drug loading, nanomedicine stability and drug release control are critical issues. To enhance drug loading and stability, micelle-forming polypeptides were grafted with doxorubicin, benzyl alcohol, and 4-phenyl-1-butanol that afford elevated hydrophobic interactions and π-π stacking [21,22], or cinnamyl, dihydroxyphenylalanine, lipoid acid, and cystine groups that stabilize nanosystems *via* chemical crosslinking [23–29]. To facilitate drug release at tumor sites, bioresponsive polypeptides have been extensively explored [30,31]. For example, pH-responsive polymeric nanoparticles developed from poly(L-histidine), poly(L-aspartate) and poly(L-glutamate) derivatives with N,N′-diethylethylenediamine,

* Corresponding authors.
E-mail addresses: zyzhong@suda.edu.cn (Z. Zhong), cdeng@suda.edu.cn (C. Deng).

https://doi.org/10.1016/j.jconrel.2019.03.005
Received 28 December 2018; Received in revised form 1 March 2019; Accepted 6 March 2019
Available online 18 March 2019
0168-3659/

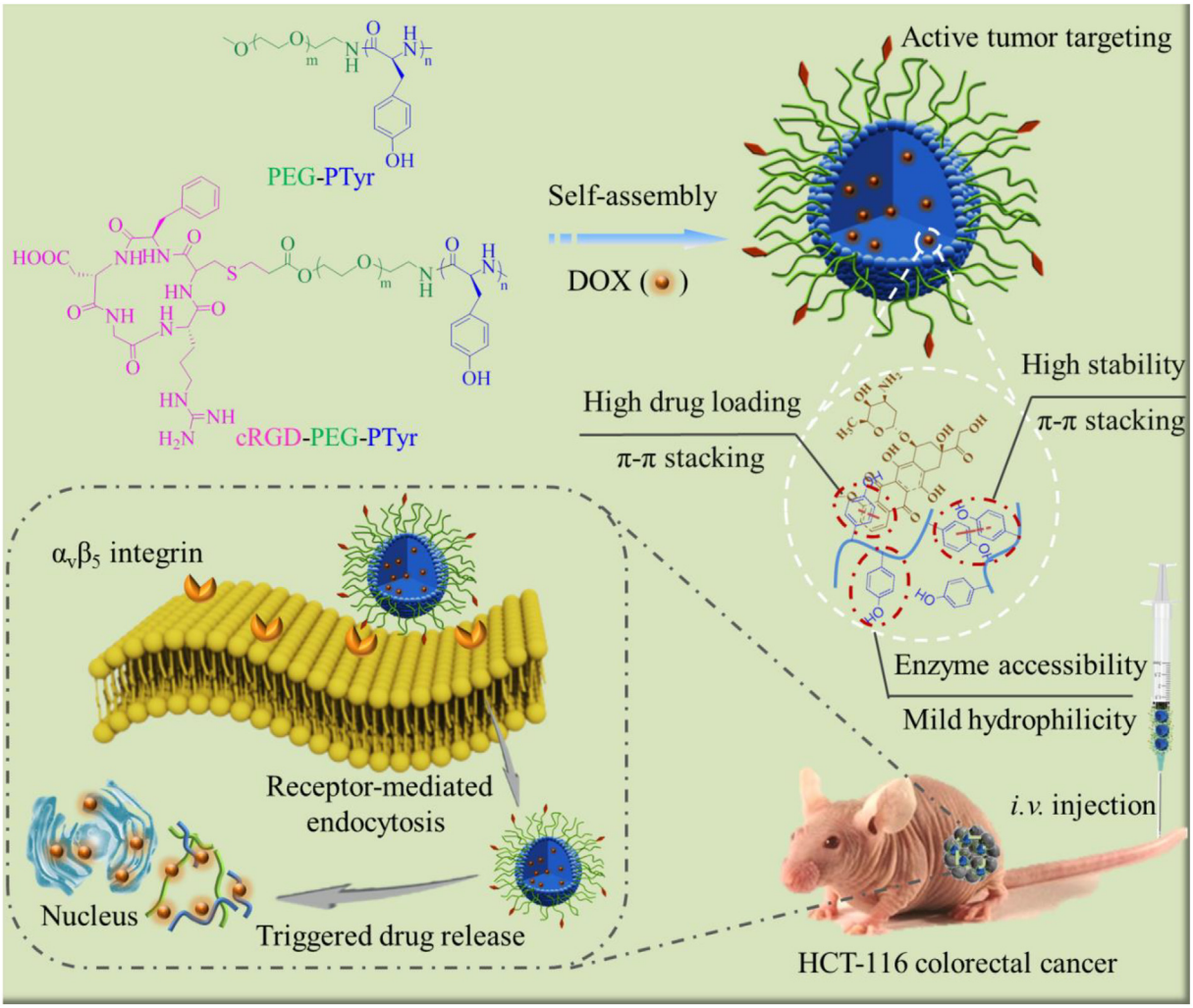

Scheme 1. Illustration of cRGD-decorated polytyrosine nanoparticles (cRGD-PTN) for robust encapsulation and targeted delivery of DOX to HCT-116 colorectal tumor in mice. cRGD-PTN is co-assembled from PEG-PTyr and cRGD-PEG-PTyr (4/1, mol/mol). DOX is efficiently and robustly encapsulated in cRGD-PTN through π-π stacking. DOX-loaded cRGD-PTN has a long circulation time, efficiently accumulates in the tumor, and is internalized by HCT-116 cells *via* receptor-mediated mechanism. In HCT-116 cells, PTyr is subject to enzymatic degradation, triggering DOX release and cell death.

histamine, and 2-(diisopropylamino) ethylamine were shown to swell and dissociate at acidic tumor environment, resulting in accelerated drug release [32–35]. Redox-responsive polypeptide nanovehicles that enhance drug release under intracellular reduction environment have been fabricated from poly(L-cystine), poly(L-cysteine), and polypeptide derivatives [36–39]. In spite of devoted work toward targeted cancer nanomedicines, no such polypeptide system has entered clinical settings to date, partially owing to the fact that designed targeted nanomedicines are too sophisticated to translate [40,41]. Interestingly, we recently found that polytyrosine nanoparticles (PTN) based on PEG-PTyr diblock copolymer are robust and display high loading and fast intracellular release of doxorubicin (DOX), which could be attributed to existence of π-π stacking and enzymatic degradation, respectively [42]. PTN provides a simple while multifunctional biodegradable vehicle for targeted cancer therapy.

Here, we report on construction of cRGD-PTN for robust encapsulation and targeted delivery of DOX to colorectal cancer *in vivo* (Scheme 1). cRGD has been extensively explored to improve nanomedicine's affinity and uptake by $\alpha_v\beta_5$ and $\alpha_v\beta_3$ integrin overexpressing cancer cells including HCT-116 colon cancer cells [43–47]. Interestingly, ^{125}I radiolabeling reveals that cRGD decoration affords 2.8-fold better accumulation of PTN in HCT-116 colon tumor in mice. cRGD-PTN-DOX shows over 5 times higher toleration compared with clinically used Lipo-DOX and induces effective inhibition of HCT-116 colorectal tumor with depleting side effects.

2. Experimental methods

2.1. Synthesis of cRGD-PEG-PTyr copolymer

Acrylated PEG-PTyr (AA-PEG-PTyr) was firstly prepared through controlled polymerization of Tyr-NCA using AA-PEG-NH_2 as an initiator, similar to a previous report [42]. cRGD-PEG-PTyr copolymer was obtained by thiol-ene reaction of AA-PEG-PTyr with cRGDfC (Fig. S1). In brief, a solution of AA-PEG-PTyr (110.0 mg, 10 μmol AA group) in DMF (2.0 mL) was added to a solution of cyclic RGDfC peptide (cRGD, 9.8 mg, 12 μmol) in DMF (1.0 mL), followed by UV irradiation (320–390 nm, 50 mW/cm^2) for 10 min in the presence of I2959 photoinitiator. The product was purified by dialysis (MWCO 7000) in D.I. water for 48 h followed by lyophilization to obtain cRGD-PEG-PTyr. Yield: 78.0%. Cy5-labeled PEG-PTyr (Cy5-PEG-PTyr) was acquired through the reaction of Cy5-NHS with terminal amino groups of PEG-PTyr.

^{125}I–labeled PEG-PTyr copolymer (^{125}I-PEG-PTyr) was obtained by the reaction of PEG-PTyr (5.0 mg, 5.1×10^{-4} mmol) with Na^{125}I in DMF (200 μL, 216 μCi) at room temperature (r.t.) for 15 min. Excess

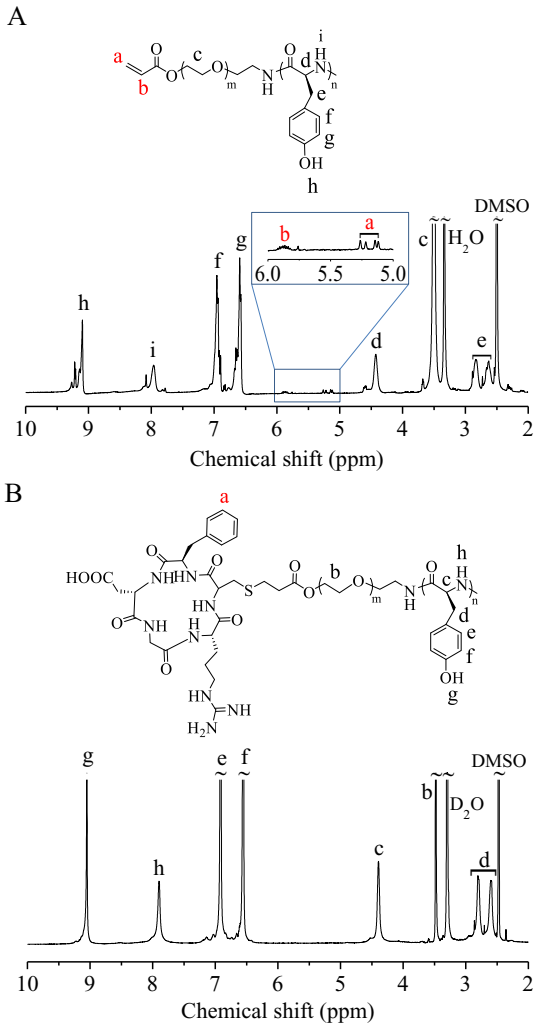

Fig. 1. ^{1}H NMR spectra (600 MHz, DMSO-d_6) of AA-PEG-PTyr (A) and cRGD-PEG-PTyr (B).

$Na^{125}I$ was removed by exhaustive dialysis (MWCO 7000 Da) in HEPES (pH 7.4, 10 mM). The radioactivity of ^{125}I-PEG-PTyr was measured by radioactivity meter (Beijing Heng Odd Instrument Co., Ltd). The efficiency of iodine exchange reaction calculated by dividing the initial radioactivity of $Na^{125}I$ with the radioactivity of ^{125}I-PEG-PTyr was 51%.

2.2. Fabrication of blank and DOX-loaded cRGD-PTN

Blank cRGD-PTN was fabricated from PEG-PTyr and cRGD-PEG-PTyr *via* solvent exchange method. Briefly, a solution (5.0 mg/mL, 100 μL) of PEG-PTyr and cRGD-PEG-PTyr mixture at a molar ratio of 4:1 in DMF was added dropwise to HEPES (10 mM, pH 7.4, 900 μL), followed by exhaustive dialysis (MWCO 7000) in HEPES. Cy5-labeled cRGD-PTN (Cy5-cRGD-PTN) was similarly prepared except that 10 mol % of Cy5-PEG-PTyr was mixed in polymer solution. ^{125}I–bearing cRGD-PTN (^{125}I-cRGD-PTN) was similarly prepared by dropwise addition of ^{125}I-PEG-PTyr and cRGD-PEG-PTyr at a molar ration of 4:1 in DMF to 900 μL of HEPES.

cRGD-PTN-DOX was fabricated by dropwise adding a DMF solution of block polymer and predetermined amount of DOX (10 mg/mL in DMSO) into the HEPES (pH 7.4, 10 mM) prior to extensive dialysis against HEPES. The solution of cRGD-PTN-DOX was diluted with DMF (30-fold) to extract the encapsulated DOX, and the amount of DOX was measured by fluorometry (ex. 480 nm, em. 560 nm). The drug loading content (DLC) and drug loading efficiency (DLE) were determined as the following:

DLC (wt%) = (weight of encapsulated DOX/total weight of polymer and encapsulated DOX) × 100.

DLE (%) = (weight of encapsulated DOX/feed weight of DOX) × 100.

2.3. In vivo biodistribution

The mice were handled under protocols approved by the Animal Care and Use Committee of Soochow University. Human HCT-116 colorectal tumor xenografts were acquired *via* subcutaneous implantation of minced colorectal tumor tissue into Balb/c nude mice. When tumor size reaching 100–200 mm^3, Cy5-PTN and Cy5-cRGD-PTN (200 μL, Cy5 concentration: 25 μg/mL) were intravenously administered into the tumor-bearing mice through the tail. A near-infrared fluorescence imaging system (Caliper IVIS Lumina II) was employed to collect the whole body Cy5 fluorescence images at predetermined time points. For *ex vivo* imaging, mice were administered with PTN-DOX and cRGD-PTN-DOX (DOX concentration: 10 mg DOX equv./kg). The tumor and major organs were harvested at 4 h post injection to acquire DOX fluorescence images.

The biodistribution and tumor targetability of cRGD-PTN was further studied using SPECT/CT. Briefly, ^{125}I-cRGD-PTN or ^{125}I-PTN with a dose of 108 μCi/kg was administered into BALB/c nude mice *via* intravenous injection when the volume of HCT-116 tumors reached about 100–200 mm^3. SPECT/CT images were collected using U-SPECT/CT (MILabs, Netherlands).

2.4. In vivo antitumor efficacy

The therapeutic effect of cRGD-PTN-DOX and PTN-DOX was assessed using nude mice bearing HCT-116 tumor. When the tumors grew up to around 100 mm^3, the mice were intravenously administrated with 4 doses of cRGD-PTN-DOX (6 or 12 mg DOX equiv./kg), PTN-DOX (6 mg DOX equiv./kg), Lipo-DOX (6 mg DOX equiv./kg), and blank cRGD-PTN every 4 days, respectively. The tumor volume was determined using the formula $V = 0.5 \times L \times W^2$ (L: tumor dimension at the longest point, W: tumor dimension at the widest point). The maximum tolerated dose (MTD) was investigated in tumor-free nude mice. Following a single intravenous injection of cRGD-PTN-DOX (60, 80 and 100 mg DOX equiv./kg) or Lipo-DOX (10 and 20 mg DOX equiv./kg), mice were observed and weighted within 7 days. The MTD was determined as the highest dose that does not lead to death, abrupt body weight loss (> 15%), and the appearance of intolerable toxicity.

2.5. Statistical analysis

Data were displayed as mean ± S.D. One-way analysis of variance (ANOVA) with Bonferroni correction was employed to assess the differences between groups. $*p < .05$, and $**p < .01$ as well as $***p < .001$ were indicated significant and highly significant, respectively.

3. Results and discussion

3.1. Synthesis of cRGD-PEG-PTyr copolymer

cRGD-PEG-PTyr copolymer was synthesized by controlled polymerization of Tyr-NCA in DMF using heterobifunctional AA-PEG-NH_2 (M_n = 6.0 kg/mol) as an initiator, followed by thiol-ene reaction with cRGDfC peptide. Fig. 1A shows the ^{1}H NMR spectrum of AA-PEG-PTyr in which characteristic signals of AA group were discerned at δ 5.12–5.26 and 5.86, PTyr at δ 9.08, 6.94, 6.58, 4.42, 2.83 and 2.64, and PEG at δ 3.51. The degree of polymerization (DP) of PTyr in AA-PEG-PTyr was calculated to be 30.0 by comparing the integrals at δ 6.58 and 3.51. AA-PEG-PTyr copolymer displayed an M_n of 13.9 kg/mol and

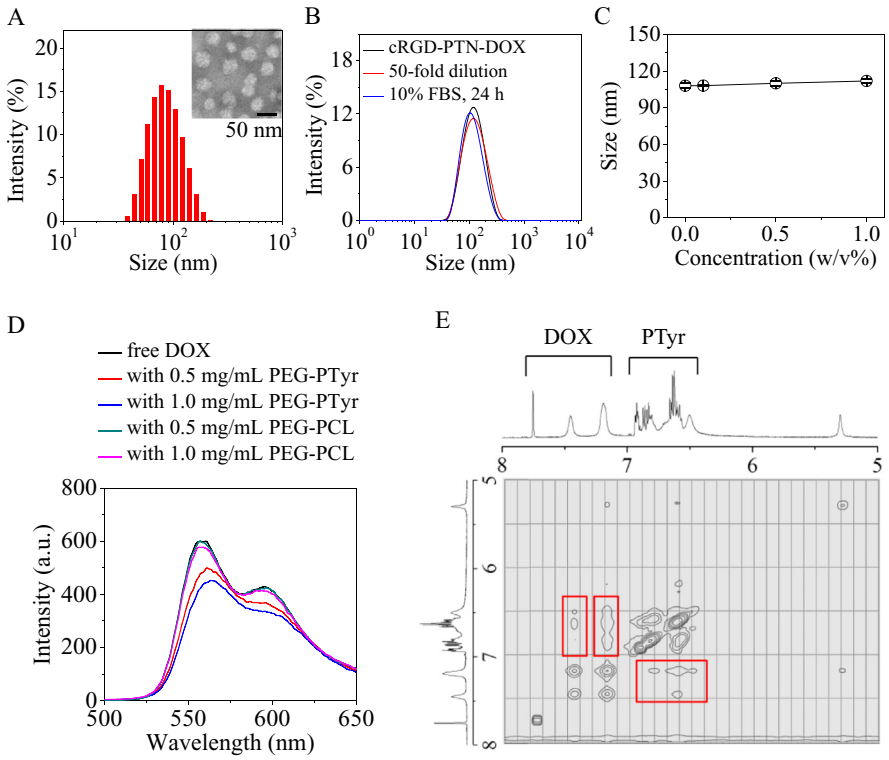

Fig. 2. (A) Size distribution of cRGD-PTN measured by DLS and TEM. (B) Colloidal stability of cRGD-PTN-DOX against dilution and 10% FBS. (C) Hydrodynamic size of cRGD-PTN-DOX as a function of concentrations of hydrophobic competitors, Triton X-100. (D) Assessment of intermolecular interactions between PEG-PTyr and free DOX (5.0 μg/mL) in DMF by fluorescence measurements. (E) ^{1}H NMR 2D nuclear Overhauser effect spectroscopy (NOESY) of PTN-DOX in D_2O (5.0–8.0 ppm).

narrow distribution (M_w/M_n = 1.09) as characterized by GPC measurements (Fig. S2). The thiol-ene reaction between AA-PEG-PTyr and cRGDfC peptide was conducted in DMF with 10 min UV irradiation. Fig. 1B showed that cRGD-PEG-PTyr possessed besides the peak of PTyr and PEG, also resonances of cRGD at δ 7.07–7.13. Meanwhile, the signals at δ 5.12–5.86 attributed to acrylate group disappeared, signifying the successful conjugation of cRGD. Using 9, 10-phenanthraquinone method [48], the degree of cRGD conjugation of cRGD-PEG-PTyr was further quantified to be 94%.

3.2. Preparation of cRGD-PTN and cRGD-PTN-DOX

The self-assembly of PEG-PTyr and cRGD-PEG-PTyr led to the formation of monodisperse nanoparticles (cRGD-PTN) possessing a mean size of 70 nm and low PDI of 0.12 (Fig. 2A). The size and size distribution was further visualized by TEM images. Upon treating with proteinase K (6 U/mL), cRGD-PTN displayed significantly enlarged size in 2 h (Fig. S3A). The fast enzymatic responsivity of cRGD-PTN could be attributed to the mild hydrophilicity of micellar core resulting from phenolic hydroxyl groups of PTyr segments, facilitating their access to enzymes. In contrast, many polypeptide-based nanoparticles with PEG shielding exhibited impeded enzymatic degradability [20,49]. Taking advantages of strong π-π stacking interactions between DOX and phenyl groups of PTyr block, cRGD-PTN displayed an extraordinary drug loading capacity with drug loading contents of 18.5–54.1 wt% (Table 1). Besides π-π stacking [50,51], several other physical strategies including electrostatic interactions [52,53], hydrogen bonding [54,55], and donor-acceptor interaction [56] have been recently introduced into polymeric nanoparticles to achieve superb loading of different drugs. DOX-loaded nanoparticles (cRGD-PTN-DOX) did not show obvious size change upon adding 10% FBS and a hydrophobic interaction competitor, Triton X-100 (Fig. 2B–C), indicating that cRGD-PTN-DOX is extraordinarily stable. The robustness of PTN-DOX and cRGD-PTN-DOX was further verified by their little size change in PBS within 7 days (Fig. S4). Fig. 2D displays that PEG-PTyr copolymer induced obvious fluorescence quenching of DOX (5.0 μg/mL) as a result of proximal intermolecular interaction between DOX and PTyr block, and the fluorescence intensities decreased with increasing concentrations of PEG-PTyr. In contrast, PEG-poly(ε-caprolactone) (PEG-PCL) displayed little fluorescence quenching for DOX under otherwise the same conditions. The quenching of DOX fluorescence implies strong intermolecular interactions between PTyr and DOX. Similar DOX fluorescence quenching was observed in coumarin, chrysin or epigallocatechin gallate (EGCG)-containing nanoparticles [51,57]. It has been reported that intermolecular interaction between paclitaxel and naphthyl-functionalized micelles could be examined through 2D NOESY NMR [58]. Using similar strategy, we further investigated the intermolecular correlation of PTN-DOX, and the results showed that there exist clear cross-peaks at δ 6.5–7.8 (Fig. 2E), corroborating the strong intermolecular π-π stacking interactions between aromatic protons of PTyr and DOX. The *in vitro* release studies revealed that about 87% of DOX was released in 24 h in PBS containing proteinase K (6 U/mL), while < 19% of DOX was released under enzyme-free conditions (Fig. S5). To explore the drug release profile in cancer cells, cRGD-PTN-DOX at a dose of 100 μg/mL of DOX was used to facilitate the accurate quantification of DOX by fluorescence measurement and avoid severe toxicity in cancer cells. The results revealed that cRGD-PTN-DOX following 10 h incubation with

Table 1
Characterization of cRGD-PTN-DOX.

Entry	DLC (wt%)		DLE[a] (%)	Size[b] (nm)	PDI[b]	Zeta[c] (mV)
	theory	determined[a]				
1	20	18.5	90.7	93	0.11	−3.2
2	30	27.0	86.3	105	0.13	−3.1
3	40	35.5	82.6	121	0.15	−3.0
4	50	44.5	80.1	129	0.18	−2.5
5	60	54.1	78.6	145	0.19	−2.2

[a] Determined by fluorescence measurement.
[b] Determined by DLS analysis.
[c] Measured by electrophoresis.

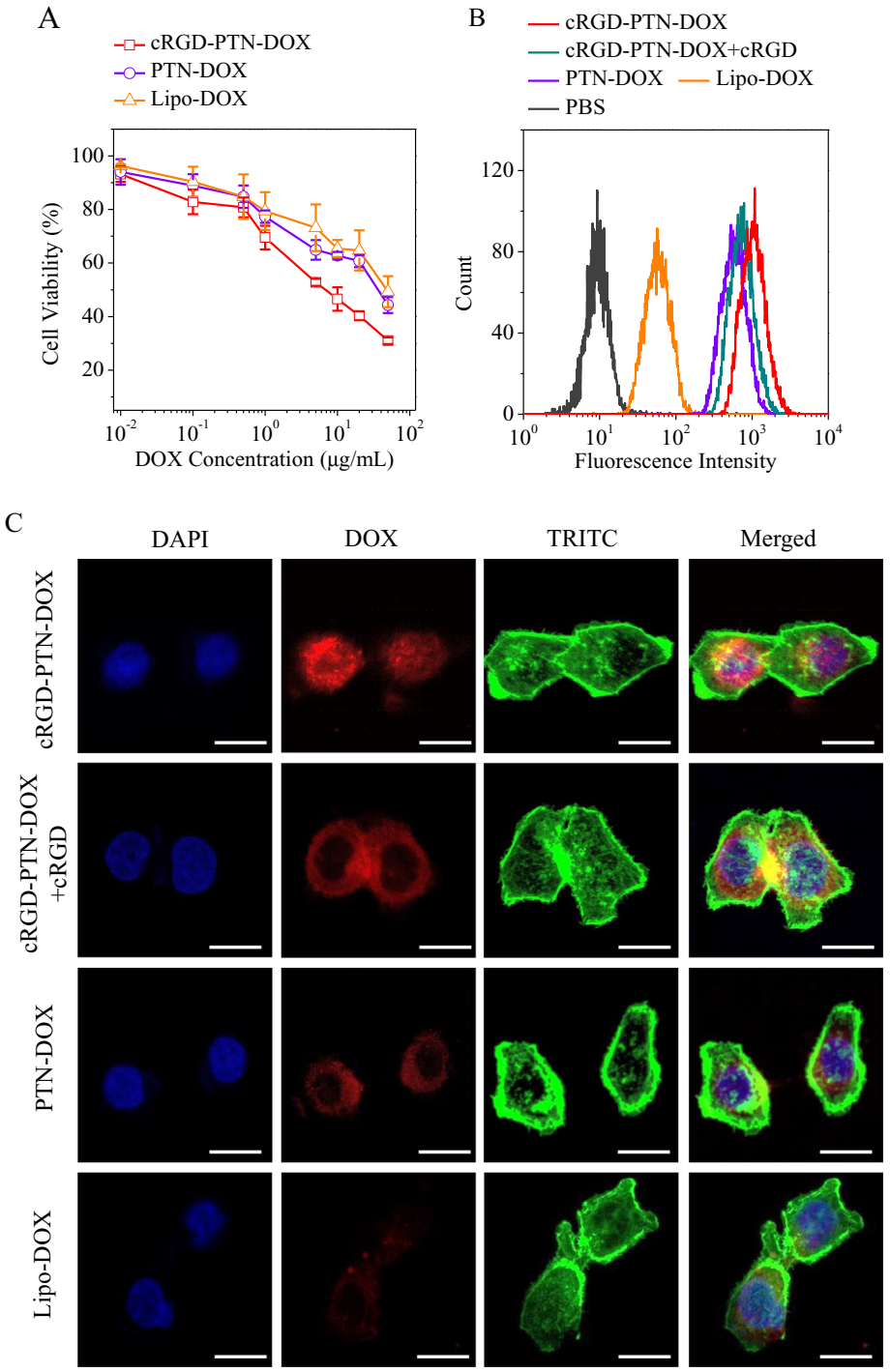

Fig. 3. (A) The antiproliferative activity of cRGD-PTN-DOX in HCT-116 cells. The cells were incubated with cRGD-PTN-DOX for 4 h, and in a fresh culture medium for another 44 h. Flow cytometry (B) and confocal laser scanning microscopy (CLSM) images (C) of HCT-116 cells treated with cRGD-PTN-DOX, PTN-DOX, and Lipo-Dox (10.0 μg DOX equiv./mL) for 4 h. Scale bar: 20 μm.

HCT-116 colorectal cancer cells exhibited nearly 90% drug release (Fig. S6). These results indicate that cRGD-PTN possesses not only robust and high encapsulation of DOX but also triggered intracellular drug release, which are both critical for targeted chemotherapy.

3.3. Selectivity and cytotoxicity of cRGD-PTN-DOX to HCT-116 cancer cells

Antiproliferation effect of cRGD-PTN-DOX was explored using MTT assays in $\alpha_v\beta_5$ integrin positive HCT-116 cells. Fig. 3A shows that cRGD-PTN-DOX exhibited remarkable cytotoxicity with a half-maximal inhibitory concentration (IC_{50}) of 6.7 μg/mL, which was 3.1-fold and 5.9-fold lower than that of the non-targeted PTN-DOX (20.8 μg/mL) and clinically used Lipo-DOX formulations (39.5 μg/mL), respectively. Noticeably, the blank PTN and cRGD-PTN were practically non-toxic, and displayed a high cell viability of over 91% at concentrations of 0.1–1.0 mg/mL (Fig. S7). While the maximum concentration of cRGD-PTN used for the anitiproliferation evaluation of cRGD-PTN-DOX (50 μg DOX equiv./mL) was 0.13 mg/mL. Besides, natural amino acid is the only degradation byproduct of cRGD-PTN, further signifying its *in vivo*

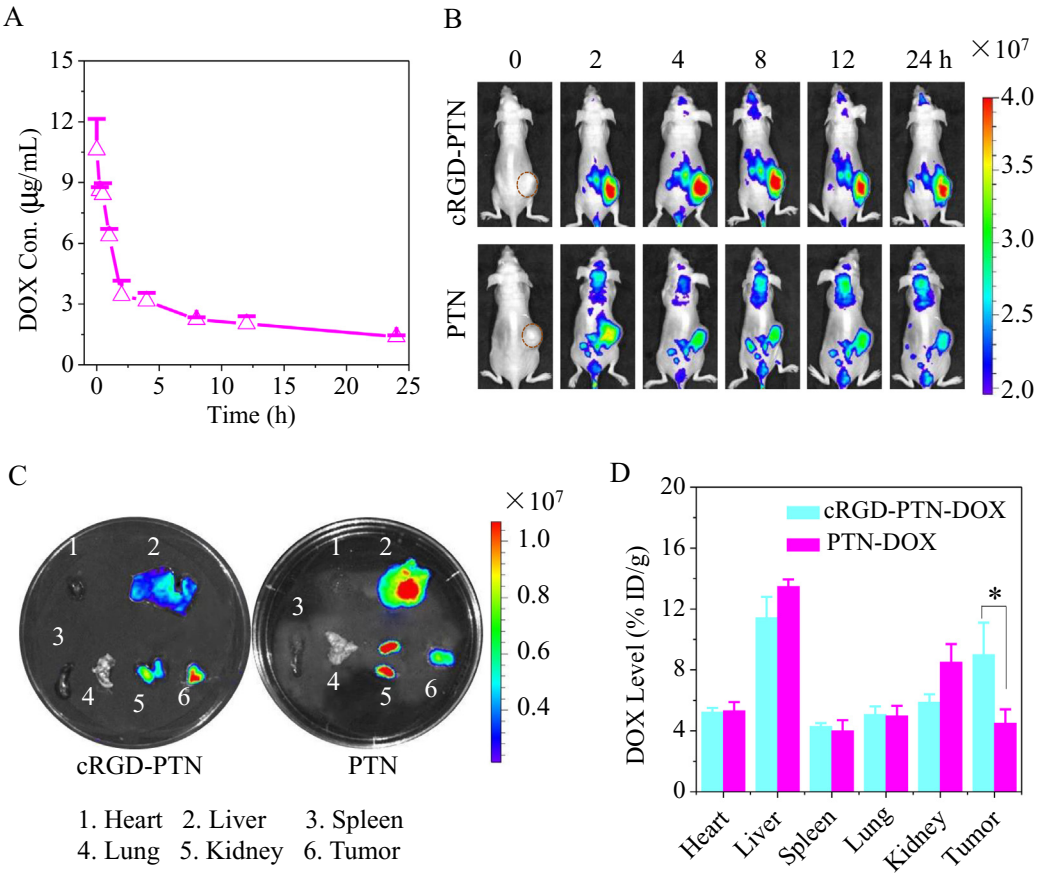

Fig. 4. *In vivo* pharmacokinetics and biodistribution studies. (A) *In vivo* pharmacokinetics of cRGD-PTN-DOX in Balb/c mice. (B) *In vivo* fluorescence images of HCT-116 tumor bearing nude mice treated with Cy5-labeled PTN and cRGD-PTN (200 μL, Cy5 concentration: 25 μg/mL). (C) DOX fluorescence images of tumors and major organs harvested from HCT-116 tumor bearing nude mice following 4 h post intravenous injection of PTN-DOX or cRGD-PTN-DOX. (D) *In vivo* biodistribution of DOX following 4 h post-injection of cRGD-PTN-DOX and PTN-DOX in HCT-116 tumor bearing nude mice ($n = 3$, $^*p < .05$).

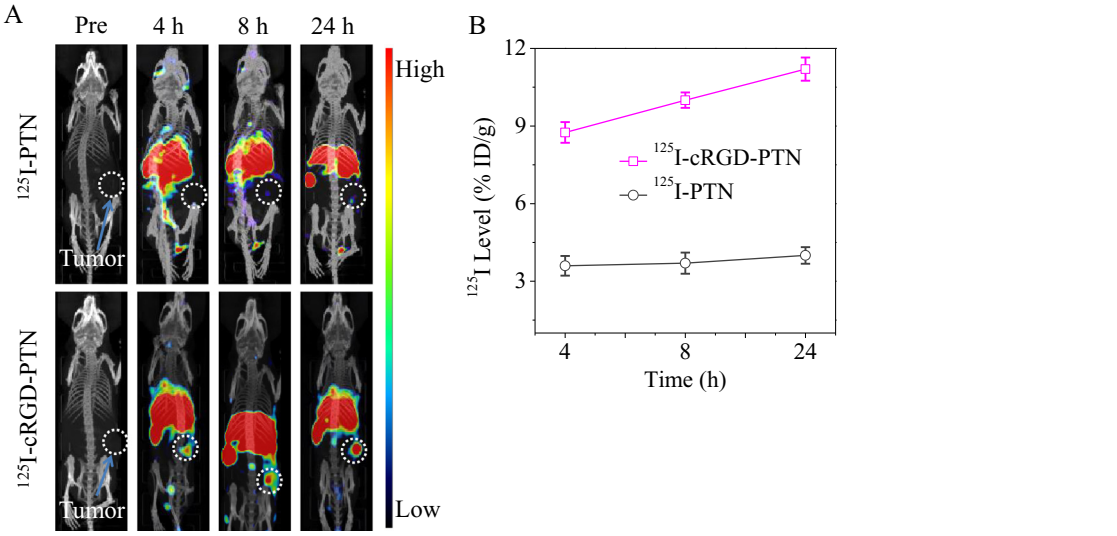

Fig. 5. (A) *In vivo* SPECT/CT images of HCT-116 colorectal tumor-bearing nude mice administered with ^{125}I-PTN and ^{125}I-cRGD-PTN. (B) Quantification of ^{125}I accumulated in tumors over time.

biocompatibility. Nanoparticles based on polypeptides possess good safety and have been broadly investigated for cancer therapy and diagnosis [59–61]. In order to explore the internalization of DOX-loaded nanoparticles, we have measured the amount of DOX in HCT-116 cancer cells following 4 h incubation with cRGD-PTN-DOX and PTN-DOX. The results showed that about 41.3% and 72.9% of DOX were internalized into HCT-116 cells with PTN-DOX and cRGD-PTN-DOX, respectively. Flow cytometry further showed that cRGD-PTN-DOX could be efficiently internalized in HCT-116 cells, and the amount of cellular uptake was around 2-fold and 18-fold higher than that of non-

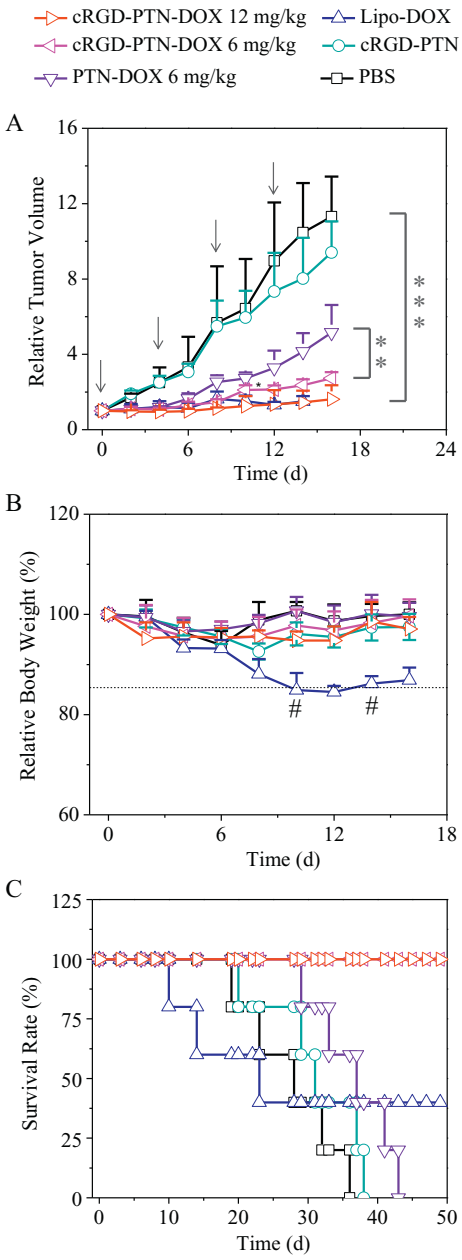

Fig. 6. *In vivo* therapeutic efficacy of cRGD-PTN-DOX. (A) Tumor volume changes of mice treated with cRGD-PTN-DOX, PTN-DOX, Lipo-DOX, cRGD-PTN and PBS, respectively (n = 6). (B) Body weight changes of mice in different treatment groups within 16 d (n = 6). "#" indicates one mouse died during treatment. (C) Survival rates of mice treated with different formulation within 50 d.

targeting counterpart (PTN-DOX) and Lipo-DOX, respectively (Fig. 3B). Pretreating HCT-116 cells with free cRGD peptide (2 mg/mL) for 4 h before adding cRGD-PTN-DOX led to clearly decreased cellular uptake, further corroborating cRGD plays an important role in the cellular uptake of cRGD-PTN-DOX. Fig. 3C exhibited that HCT-116 cells treated with cRGD-PTN-DOX revealed strong DOX fluorescence in the nuclei, suggesting that cRGD-PTN-DOX could efficiently target to $\alpha_v\beta_5$ over-expressing cancer cells and achieve fast intracellular drug release. In contrast, PTN-DOX and Lipo-DOX revealed much weaker DOX fluorescence and most DOX was located in the cytoplasm under otherwise the same conditions. The different distribution of DOX in HCT-116 cells could be attributed that cRGD-PTN-DOX had higher and faster cellular uptake *via* $\alpha_v\beta_5$ integrin-mediated internalization in comparison with

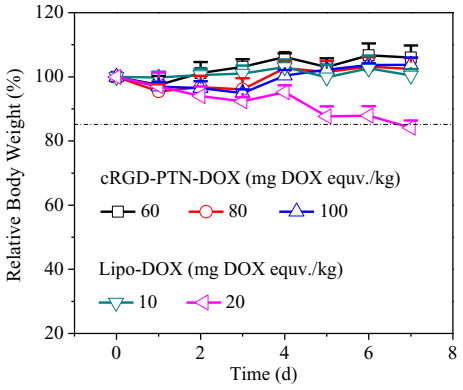

Fig. 7. Maximum-tolerated dose (MTD) evaluated by measuring the body weight changes of Balb/c mice intravenously administrated with a single injection of cRGD-PTN-DOX and Lipo-DOX within 7 d.

PTN-DOX, which has been also observed in A549 and U87 cancer cells treated with cRGD-decorated micelles and polymersomes [44,62]. As expected, pretreating HCT-116 cells with free cRGD significantly reduced DOX fluorescence in the nuclei. These results confirm that cRGD-PTN-DOX can actively target to HCT-116 cells and quickly release DOX into the nuclei, giving high antitumor activity to HCT-116 cells.

3.4. *In vivo* pharmacokinetics and biodistribution

The *in vivo* pharmacokinetics was explored by measuring the plasma DOX levels of mice administrated with a single dose of cRGD-PTN-DOX. Noticeably, cRGD-PTN-DOX exhibited an extended blood circulation time with an elimination phase half-life of 3.12 h (Fig. 4A), in comparison with free DOX and many reported non-crosslinked nanoparticles [63,64]. The prolonged blood circulation time of cRGD-PTN-DOX could attribute to their high stability conferred by π-π stacking interactions between drug and PTyr moieties. To visualize the *in vivo* tumor-targeting effect, HCT-116 bearing nude mice were administered intravenously with Cy5-labeled cRGD-PTN and PTN, and then imaged using a near-infrared fluorescence imaging system. Fig. 4B showed that cRGD-PTN group presented significant Cy5 fluorescence in the tumor at 2 h post injection, and the fluorescence intensity was elevated at 4–8 h and remained sharp even at 24 h. In comparison, mice treated with Cy5-labled PTN displayed much weaker Cy5 fluorescence at the same experimental period. Moreover, mice treated with cRGD-PTN-DOX exhibited much stronger DOX fluorescence in tumor than any other organs (Fig. 4C), corroborating that cRGD-PTN has good tumor selectivity. In contrast, PTN-DOX group exhibited clearly weaker DOX fluorescence in tumor, while strongest DOX fluorescence in the liver and kidney. We further quantified DOX distributed in tumor and normal tissues at 4 h post-injection of cRGD-PTN-DOX. The results revealed a boosted tumor DOX accumulation of 9% ID/g, which was around two times higher than that for PTN-DOX (Fig. 4D).

Taking advantages of facile substitution of ortho-H of tyrosine with radioactive iodine [65–67], we prepared ^{125}I-labeled PTN and cRGD-PTN to monitor their *in vivo* biodistribution and tumor targetability by SPECT. ^{125}I-labeled PEG-PTyr was easily obtained by iodine exchange reaction with an efficiency of 51%. Fig. 5A shows clearly that ^{125}I-cRGD-PTN gave markedly enhanced accumulation in the HCT-116 colorectal tumor than non-targeted ^{125}I-PTN. The tumor accumulation increased from 4 to 24 h post-injection. The quantification of radioactivity reveals that ^{125}I-cRGD-PTN afforded a high tumor accumulation of 11.2% ID/g at 24 h, which was 2.8-fold higher than ^{125}I-PTN (Fig. 5 B).

3.5. In vivo therapeutic efficacy

The *in vivo* antitumor activity of cRGD-PTN-DOX was evaluated using HCT-116 tumor-bearing nude mice. cRGD-PTN-DOX was observed to significantly inhibit tumor growth at a dosage of 6 mg/kg, which was significantly better than PTN-DOX ($p < .01$) (Fig. 6A), supporting that cRGD peptide can actively target to HCT-116 tumor. Increasing the dosage of cRGD-PTN-DOX to 12 mg DOX equiv./kg afforded nearly complete suppression of tumor growth. The images of tumors harvested on day 16 revealed that mice administered with 12 mg DOX equiv./kg cRGD-PTN-DOX exhibited the smallest tumor size (Fig. S8). Noticeably, mice following the treatment with cRGD-PTN-DOX at both high and low dosages revealed negligible body weight loss (Fig. 6B), suggesting that DOX encapsulated in cRGD-PTN generated little systemic toxicity. In contrast, Lipo-DOX group exhibited obvious body weight loss (> 15%) and even death from day 10. Besides, mice treated with cRGD-PTN-DOX at both 6 and 12 mg DOX equiv./kg all survived within the experimental period of 50 d, while Lipo-DOX, PTN-DOX, blank cRGD-PTN and PBS groups displayed median survival times of 23 d, 37 d, 31 d and 28 d, respectively (Fig. 6C). cRGD-PTN-DOX was observed to generate significant tumor cell necrosis as a characterization of nuclei lysis (Fig. S9), but little damage to healthy organs (Fig. S10). Lipo-DOX though induced cell death at tumor sites also instigated obvious side effect including significant hepatotoxicity. Maximum-tolerated dose (MTD) measurement exhibited that cRGD-PTN-DOX displayed a remarkably high MTD (> 100 mg DOX equiv./kg), in sharp contrast with the low MTD of Lipo-DOX (< 20 mg DOX equiv./kg) (Fig. 7). The remarkably high MTD of cRGD-PTN-DOX likely resulted from its high stability, minimum drug leakage, elevated biodistribution and favorable cellular uptake. cRGD-PTN-DOX with potent therapeutic efficacy, enlarged therapeutic window, and little systemic toxicity holds a great potential in clinical translation.

4. Conclusions

We have demonstrated that cRGD-decorated polytyrosine nanoparticles (cRGD-PTN) are a simple and yet multifunctional biodegradable nanovehicle that possesses not only a high encapsulation of doxorubicin (DOX, 18.5–54.1 wt%), superb stability, extended blood circulation time, and triggered drug release inside cancer cells, but also high selectivity toward HCT-116 colorectal cancer cells and significantly improved tumor accumulation in comparison with the non-targeted PTN control. Interestingly, cRGD-PTN-DOX exhibits over 5 times better toleration than clinically used liposomal DOX formulation. The therapeutic studies reveal that cRGD-PTN-DOX can effectively inhibit growth of HCT-116 colorectal tumor at 6 or 12 mg DOX equiv./kg without causing pronounced systemic toxicity, leading to markedly improved survival rate in HCT-116 tumor-bearing mice. The great simplicity, good safety and multi-functionality of cRGD-PTN make it a truly unique and appealing platform for clinical translation.

Acknowledgments

This work was supported by the National Natural Science Foundation of China (NSFC 51773145, 51473110, 51633005, and 51761135117).

Appendix A. Supplementary data

Supplementary data to this article can be found online at https://doi.org/10.1016/j.jconrel.2019.03.005.

References

[1] A. Kreso, P. van Galen, N.M. Pedley, E. Lima-Fernandes, C. Frelin, T. Davis, L.X. Cao, R. Baiazitov, W. Du, N. Sydorenko, Y.C. Moon, L. Gibson, Y.D. Wang, C. Leung, N.N. Iscove, C.H. Arrowsmith, E. Szentgyorgyi, S. Gallinger, J.E. Dick, C.A. O'Brien, Self-renewal as a therapeutic target in human colorectal cancer, Nat. Med. 20 (2014) 29–36.
[2] C.J.A. Punt, M. Koopman, L. Vermeulen, From tumour heterogeneity to advances in precision treatment of colorectal cancer, Nat. Rev. Clin. Oncol. 14 (2017) 235–246.
[3] S. Manfredi, A.M. Bouvier, C. Lepage, C. Hatem, V. Dancourt, J. Faivre, Incidence and patterns of recurrence after resection for cure of colonic cancer in a well defined population, Br. J. Surg. 93 (2006) 1115–1122.
[4] T.D. Christensen, K.L.G. Spindler, J.A. Palshof, D.L. Nielsen, Systematic review: brain metastases from colorectal cancer-incidence and patient characteristics, BMC Cancer 16 (2016) 260.
[5] C. Eng, Toxic effects and their management: daily clinical challenges in the treatment of colorectal cancer, Nat. Rev. Clin. Oncol. 6 (2009) 207–218.
[6] H. Xiao, L. Yan, E.M. Dempsey, W. Song, R. Qi, W. Li, Y. Huang, X. Jing, D. Zhou, J. Ding, X. Chen, Recent progress in polymer-based platinum drug delivery systems, Prog. Polym. Sci. 87 (2018) 70–106.
[7] J. Shi, P.W. Kantoff, R. Wooster, O.C. Farokhzad, Cancer nanomedicine: progress, challenges and opportunities, Nat. Rev. Cancer 17 (2017) 20–37.
[8] A. Varela-Moreira, Y. Shi, M.H.A.M. Fens, T. Lammers, W.E. Hennink, R.M. Schiffelers, Clinical application of polymeric micelles for the treatment of cancer, Mater. Chem. Front. 1 (2017) 1485–1501.
[9] Y.S. Youn, Y.H. Bae, Perspectives on the past, present, and future of cancer nanomedicine, Adv. Drug Deliv. Rev. 130 (2018) 3–11.
[10] B. Chibaudel, F. Maindrault-Goebel, J.-B. Bachet, C. Louvet, A. Khalil, O. Dupuis, P. Hammel, M.-L. Garcia, M. Bennamoun, D. Brusquant, C. Tournigand, T. Andre, C. Arbaud, A.K. Larsen, Y.-W. Wang, C.G. Yeh, F. Bonnetain, A. de Gramont, PEPCOL: a GERCOR randomized phase II study of nanoliposomal irinotecan PEP02 (MM-398) or irinotecan with leucovorin/5-fluorouracil as second-line therapy in metastatic colorectal cancer, Cancer Med 5 (2016) 676–683.
[11] K.K. Sankhala, A.C. Mita, R. Adinin, L. Wood, M. Beeram, S. Bullock, N. Yamagata, K. Matsuno, T. Fujisawa, A. Phan, A phase I pharmacokinetic (PK) study of MBP-426, a novel liposome encapsulated oxaliplatin, J. Clin. Oncol. 27 (2009) 2535.
[12] L. Belfiore, D.N. Saunders, M. Ranson, K.J. Thurecht, G. Storm, K.L. Vine, Towards clinical translation of ligand-functionalized liposomes in targeted cancer therapy: challenges and opportunities, J. Control. Release 277 (2018) 1–13.
[13] A. Alibakhshi, F.A. Kahaki, S. Ahangarzadeh, H. Yaghoobi, F. Yarian, R. Arezumand, J. Ranjbari, A. Mokhtarzadeh, M. de la Guardia, Targeted cancer therapy through antibody fragments-decorated nanomedicines, J. Control. Release 268 (2017) 323–334.
[14] Y. Zhong, F. Meng, C. Deng, Z. Zhong, Ligand-directed active tumor-targeting polymeric nanoparticles for cancer chemotherapy, Biomacromolecules 15 (2014) 1955–1969.
[15] T. Ojha, V. Pathak, Y. Shi, W.E. Hennink, C.T.W. Moonen, G. Storm, F. Kiessling, T. Lammers, Pharmacological and physical vessel modulation strategies to improve EPR-mediated drug targeting to tumors, Adv. Drug Deliv. Rev. 119 (2017) 44–60.
[16] Z. Tang, C. He, H. Tian, J. Ding, B.S. Hsiao, B. Chu, X. Chen, Polymeric nanostructured materials for biomedical applications, Prog. Polym. Sci. 60 (2016) 86–128.
[17] Z.Y. Song, Z.Y. Han, S.X. Lv, C.Y. Chen, L. Chen, L.C. Yin, J.J. Cheng, Synthetic polypeptides: from polymer design to supramolecular assembly and biomedical application, Chem. Soc. Rev. 46 (2017) 6570–6599.
[18] H. Cabral, K. Miyata, K. Osada, K. Kataoka, Block copolymer micelles in nanomedicine applications, Chem. Rev. 118 (2018) 6844–6892.
[19] G. Chen, Y. Wang, R. Xie, S. Gong, A review on core-shell structured unimolecular nanoparticles for biomedical applications, Adv. Drug Deliv. Rev. 130 (2018) 58–72.
[20] C. Deng, J.T. Wu, R. Cheng, F.H. Meng, H.A. Klok, Z.Y. Zhong, Functional polypeptide and hybrid materials: precision synthesis via alpha-amino acid N-carboxyanhydride polymerization and emerging biomedical applications, Prog. Polym. Sci. 39 (2014) 330–364.
[21] H. Cabral, K. Kataoka, Progress of drug-loaded polymeric micelles into clinical studies, J. Control. Release 190 (2014) 465–476.
[22] B.F. Sun, C. Deng, F.H. Meng, J. Zhang, Z.Y. Zhong, Robust, active tumor-targeting and fast bioresponsive anticancer nanotherapeutics based on natural endogenous materials, Acta Biomater. 45 (2016) 223–233.
[23] J. Ding, X. Zhuang, C. Xiao, Y. Cheng, L. Zhao, C. He, Z. Tang, X. Chen, Preparation of photo-cross-linked ph-responsive polypeptide nanogels as potential carriers for controlled drug delivery, J. Mater. Chem. 21 (2011) 11383–11391.
[24] L. Yan, L. Yang, H. He, X. Hu, Z. Xie, Y. Huang, X. Jing, Photo-cross-linked mPEG-poly(gamma-cinnamyl-l-glutamate) micelles as stable drug carriers, Polym. Chem. 3 (2012) 1300–1307.
[25] E.P. Holowka, T.J. Deming, Synthesis and cross linking of L-DOPA containing polypeptide vesicles, Macromol. Biosci. 10 (2010) 496–502.
[26] K. Klinker, O. Schaefer, D. Huesmann, T. Bauer, L. Capeloa, L. Braun, N. Stergiou, M. Schinnerer, A. Dirisala, K. Miyata, K. Osada, H. Cabral, K. Kataoka, M. Barz, Secondary-structure-driven self-assembly of reactive polypept(o)ides: controlling size, shape, and function of core cross-linked nanostructures, Angew. Chem. Int. Ed. 56 (2017) 9608–9613.
[27] S. Xue, X. Gu, J. Zhang, H. Sun, C. Deng, Z. Zhong, Construction of small-sized, robust and reduction-responsive polypeptide micelles for high loading and targeted delivery of chemotherapeutics, Biomacromolecules 19 (2018) 3586–3593.
[28] T. Chen, M. Qiu, J. Zhang, H. Sun, C. Deng, Z. Zhong, Integrated multifunctional micelles co-self-assembled from polypeptides conjugated with natural ferulic acid and lipoic acid for doxorubicin delivery, Chemphyschem 19 (2018) 2070–2077.
[29] H. Guo, W. Xu, J. Chen, L. Yan, J. Ding, Y. Hou, X. Chen, Positively charged polypeptide nanogel enhances mucoadhesion and penetrability of 10-hydroxycamptothecin in orthotopic bladder carcinoma, J. Control. Release 259 (2017)

136–148.
[30] Y. Shen, X. Fu, W. Fu, Z. Li, Biodegradable stimuli-responsive polypeptide materials prepared by ring opening polymerization, Chem. Soc. Rev. 44 (2015) 612–622.
[31] Z. Jiang, J. Chen, L. Cui, X. Zhuang, J. Ding, X. Chen, Advances in stimuli-responsive polypeptide nanogels, Small 2 (2018) (1700307).
[32] L. Zhang, T. Yin, B. Li, R. Zheng, C. Qiu, K.S. Lam, Q. Zhang, X. Shuai, Size-modulable nanoprobe for high-performance ultrasound imaging and drug delivery against cancer, ACS Nano 12 (2018) 3449–3460.
[33] T.-W. Wang, C.-W. Yeh, C.-H. Kuan, L.-W. Wang, L.-H. Chen, H.-C. Wu, J.-S. Sun, Tailored design of multifunctional and programmable pH-responsive self-assembling polypeptides as drug delivery nanocarrier for cancer therapy, Acta Biomater. 58 (2017) 54–66.
[34] T. Ramasamy, H.B. Ruttala, N. Chitrapriya, B.K. Poudal, J.Y. Choi, S.T. Kim, Y.S. Youn, S.K. Ku, H.-G. Choi, C.S. Yong, J.O. Kim, Engineering of cell microenvironment-responsive polypeptide nanovehicle co-encapsulating a synergistic combination of small molecules for effective chemotherapy in solid tumors, Acta Biomater. 48 (2017) 131–143.
[35] M.A. Quadir, S.W. Morton, L.B. Mensah, K. Shopsowitz, J. Dobbelaar, N. Effenberger, P.T. Hammond, Ligand-decorated click polypeptide derived nanoparticles for targeted drug delivery applications, Nanomedicine: NBM 13 (2017) 1797–1808.
[36] H.-C. Yen, H. Cabral, P. Mi, K. Toh, Y. Matsumoto, X. Liu, H. Koori, A. Kim, K. Miyazaki, Y. Miura, N. Nishiyama, K. Kataoka, Light-induced cytosolic activation of reduction-sensitive camptothecin-loaded polymeric micelles for spatiotemporally controlled in vivo chemotherapy, ACS Nano 8 (2014) 11591–11602.
[37] J. Chen, J. Ding, Y. Wang, J. Cheng, S. Ji, X. Zhuang, X. Chen, Sequentially responsive shell-stacked nanoparticles for deep penetration into solid tumors, Adv. Mater. 29 (2017) 1701170.
[38] L. Liu, H. Yi, H. He, H. Pan, L. Cai, Y. Ma, Tumor associated macrophage-targeted microrna delivery with dual-responsive polypeptide nanovectors for anti-cancer therapy, Biomaterials 134 (2017) 166–179.
[39] J. Chen, J. Ding, W. Xu, T. Sun, H. Xiao, X. Zhuang, X. Chen, Receptor and microenvironment dual-recognizable nanogel for targeted chemotherapy of highly metastatic malignancy, Nano Lett. 17 (2017) 4526–4533.
[40] V.J. Venditto, F.C. Szoka Jr., Cancer nanomedicines: so many papers and so few drugs, Adv. Drug Deliv. Rev. 65 (2013) 80–88.
[41] K. Raemdonck, S.C. De Smedt, Lessons in simplicity that should shape the future of drug delivery, Nat. Biotechnol. 33 (2015) 1026–1027.
[42] X. Gu, M. Qiu, H. Sun, J. Zhang, L. Cheng, C. Deng, Z. Zhong, Polytyrosine nanoparticles enable ultra-high loading of doxorubicin and rapid enzyme-responsive drug release, Biomater. Sci. 6 (2018) 1526–1534.
[43] L. Martinez-Jothar, S. Doulkeridou, R.M. Schiffelers, J.S. Torano, S. Oliveira, C.F. van Nostrum, W.E. Hennink, Insights into maleimide-thiol conjugation chemistry: conditions for efficient surface functionalization of nanoparticles for receptor targeting, J. Control. Release 282 (2018) 101–109.
[44] S. Quader, X. Liu, Y. Chen, P. Mi, T. Chida, T. Ishii, Y. Miura, N. Nishiyama, H. Cabral, K. Kataoka, cRGD peptide-installed epirubicin-loaded polymeric micelles for effective targeted therapy against brain tumors, J. Control. Release 258 (2017) 56–66.
[45] Y. Wang, K. Zhou, G. Huang, C. Hensley, X. Huang, X. Ma, T. Zhao, B.D. Sumer, R.J. DeBerardinis, J. Gao, A nanoparticle-based strategy for the imaging of a broad range of tumours by nonlinear amplification of microenvironment signals, Nat. Mater. 13 (2014) 204–212.
[46] M. Qiu, X. Wang, H. Sun, J. Zhang, C. Deng, Z. Zhong, Cyclic RGD-peptide-functionalized polylipopeptide micelles for enhanced loading and targeted delivery of monomethyl auristatin E, Mol. Pharm. 15 (2018) 4854–4861.
[47] K. Shen, D. Li, J. Guan, J. Ding, Z. Wang, J. Gu, T. Liu, X. Chen, Targeted sustained delivery of antineoplastic agent with multicomponent polylactide stereocomplex micelle, Nanomedicine: NBM 13 (2017) 1279–1288.
[48] N. Graf, D.R. Bielenberg, N. Kolishetti, C. Muus, J. Banyard, O.C. Farokhzad, S.J. Lippard, Alpha(v)beta(3) integrin-targeted PLGA-PEG nanoparticles for enhanced anti-tumor efficacy of a Pt(IV) prodrug, ACS Nano 6 (2012) 4530–4539.
[49] M. Qiu, J. Ouyang, H.L. Sun, F.H. Meng, R. Cheng, J. Zhang, L. Cheng, Q. Lan, C. Deng, Z.Y. Zhong, Biodegradable micelles based on poly(ethylene glycol)-b-polylipopeptide copolymer: a robust and versatile nanoplatform for anticancer drug delivery, ACS Appl. Mater. Interfaces 9 (2017) 27587–27595.
[50] Y. Shi, R. van der Meel, B. Theek, E.O. Blenke, E.H.E. Pieters, M. Fens, J. Ehling, R.M. Schiffelers, G. Storm, C.F. van Nostrum, T. Lammers, W.E. Hennink, Complete regression of xenograft tumors upon targeted delivery of paclitaxel via pi-pi stacking stabilized polymeric micelles, ACS Nano 9 (2015) 3740–3752.
[51] Y. Liang, X. Deng, L.G. Zhang, X.Y. Peng, W.X. Gao, J. Cao, Z.W. Gu, B. He, Terminal modification of polymeric micelles with pi-conjugated moieties for efficient anticancer drug delivery, Biomaterials 71 (2015) 1–10.
[52] J. Leong, W. Chin, X. Ke, S. Gao, H. Kong, J.L. Hedrick, Y.Y. Yang, Disease-directed design of biodegradable polymers: reactive oxygen species and pH-responsive micellar nanoparticles for anticancer drug delivery, Nanomedicine: NBM 14 (2018) 2666–2677.
[53] L. Wu, Y. Zou, C. Deng, R. Cheng, F. Meng, Z. Zhong, Intracellular release of doxorubicin from core-crosslinked polypeptide micelles triggered by both pH and reduction conditions, Biomaterials 34 (2013) 5262–5272.
[54] Y. Li, J. Ding, J. Zhu, H. Tian, X. Chen, Photothermal effect-triggered drug release from hydrogen bonding-enhanced polymeric micelles, Biomacromolecules 19 (2018) 1950–1958.
[55] H. Cheng, Y.-J. Cheng, S. Bhasin, J.-Y. Zhu, X.-D. Xu, R.-X. Zhuo, X.-Z. Zhang, Complementary hydrogen bonding interaction triggered co-assembly of an amphiphilic peptide and an anti-tumor drug, Chem. Commun. 51 (2015) 6936–6939.
[56] S. Lv, Y. Wu, K. Cai, H. He, Y. Li, M. Lan, X. Chen, J. Cheng, L. Yin, High drug loading and sub-quantitative loading efficiency of polymeric micelles driven by donor-receptor coordination interactions, J. Am. Chem. Soc. 140 (2018) 1235–1238.
[57] K. Liang, J.E. Chung, S.J. Gao, N. Yongvongsoontorn, M. Kurisawa, Highly augmented drug loading and stability of micellar nanocomplexes composed of doxorubicin and poly(ethylene glycol)-green tea catechin conjugate for cancer therapy, Adv. Mater. 30 (2018) 1706963.
[58] Y. Shi, M.J. van Steenbergen, E.A. Teunissen, L. Novo, S. Gradmann, M. Baldus, C.F. van Nostrum, W.E. Hennink, Pi-pi stacking increases the stability and loading capacity of thermosensitive polymeric micelles for chemotherapeutic drugs, Biomacromolecules 14 (2013) 1826–1837.
[59] T.J. Deming, Synthesis of side-chain modified polypeptides, Chem. Rev. 116 (2016) 786–808.
[60] C. He, X. Zhuang, Z. Tang, H. Tian, X. Chen, Stimuli-sensitive synthetic polypeptide-based materials for drug and gene delivery, Adv. Healthc. Mater. 1 (2012) 48–78.
[61] E. Liarou, S. Varlas, D. Skoulas, C. Tsimblouli, E. Sereti, K. Dimas, H. Iatrou, Smart polymersomes and hydrogels from polypeptide-based polymer systems through alpha-amino acid N-carboxyanhydride ring-opening polymerization. From chemistry to biomedical applications, Prog. Polym. Sci. 83 (2018) 28–78.
[62] M. Qiu, H. Sun, F. Meng, R. Cheng, J. Zhang, C. Deng, Z. Zhong, Lipopepsomes: a novel and robust family of nano-vesicles capable of highly efficient encapsulation and tumor-targeted delivery of doxorubicin hydrochloride in vivo, J. Control. Release 272 (2018) 107–113.
[63] S.C. Owen, D.P.Y. Chan, M.S. Shoichet, Polymeric micelle stability, Nano Today 7 (2012) 53–65.
[64] X.Y. Ke, D.J. Coady, C. Yang, A.C. Engler, J.L. Hedrick, Y.Y. Yang, pH-sensitive polycarbonate micelles for enhanced intracellular release of anticancer drugs: a strategy to circumvent multidrug resistance, Polym. Chem. 5 (2014) 2621–2628.
[65] E.A. Simone, B.J. Zern, A.M. Chacko, J.L. Mikitsh, E.R. Blankemeyer, S. Muro, R.V. Stan, V.R. Muzykantov, Endothelial targeting of polymeric nanoparticles stably labeled with the PET imaging radioisotope iodine-124, Biomaterials 33 (2012) 5406–5413.
[66] G.F. Sun, T. Wang, X. Li, D.N. Li, Y. Peng, X.K. Wang, G.R. Jia, W.W. Su, C. Cheng, J. Yang, C.J. Zuo, Sub-micrometer Au@PDA-I-125 particles as theranostic embolism beads for radiosensitization and SPECT/CT monitoring, Adv. Healthc. Mater. 7 (2018) 10.
[67] L. Tang, C. Peng, B. Tang, Z. Li, X. Wang, J. Li, F. Gao, L. Huang, D. Xu, P. Zhang, R. Zhuang, X. Su, X. Chen, X. Zhang, Radioiodinated small-molecule tyrosine kinase inhibitor for Her2-selective SPECT imaging, J. Nucl. Med. 59 (2018) 1386–1391.